J. Sens. Sens. Syst., 15, 209–224, 2026
https://doi.org/10.5194/jsss-15-209-2026
© Author(s) 2026. This work is distributed under
the Creative Commons Attribution 4.0 License.

JSSS Journal of Sensors and Sensor Systems Open Access

Calibration of digital cameras for remote measurements of luminance and illuminance of object surfaces

Valentyn Sudomyr and Yaroslav Osadtsa

Department of Electrical Engineering, Ternopil Ivan Puluj National Technical University, 46025 Ternopil, Ukraine

Correspondence: Valentyn Sudomyr (exopuf@gmail.com)

Received: 30 June 2026 – Revised: 2 October 2026 – Accepted: 9 November 2026 – Published: 26 November 2026

Abstract. A method for calibrating commercial digital cameras for the remote measurement of the luminance and illuminance of object surfaces is presented in this paper. Traditional photometric methods based on sequential point measurements by luminance meters and lux meters are labour intensive, whereas the proposed approach makes it possible to create two-dimensional maps of the distribution of lighting parameters within the entire frame very quickly. The method is based on the application of unprocessed raw image data to ensure the linearity of the image sensor response and to avoid nonlinear transformations performed by the camera's built-in processor. The processing included conversion of the data into CIE 1931 XYZ colour space, where the Y coordinate directly corresponds to the pixel luminance. A Canon EOS 1000D camera was used in this investigation. Calibration of this camera was carried out using semiconductor light sources with three colour temperatures (from 3053 to 7198 K) within the luminance range from 3.5 to 21.6 cd m^{-2}. It is determined that in order to ensure the required accuracy, separate calibration models (in the form of the dependence of the Y coordinate on exposure) should be applied for each value of the aperture number. The resulting models demonstrated high approximation quality ($R^2 > 0.994$). Verification on a diffuse-reflective surface showed an average deviation of 10.47 % for a sample of 21 525 control areas for first experimental dataset and an average deviation of 9.48 % for a sample of 2277 control areas for a second experimental dataset. Meanwhile, within the optimal range of the normalised signal ($Y = 0.1$–0.4), the accuracy was higher when using models for each aperture value. The developed technology makes it possible to transform the common camera into an effective two-dimensional measuring tool for remote measurements of the object luminance and illuminance.

1 Introduction

In order to evaluate the distribution of luminance or illuminance within the required observation area, it is necessary to carry out a large number of measurements at different points. The application of traditional measurement methods using luminance meters and lux meters, which allow only sequential point measurements, is extremely labour- and time-consuming in such cases (Hanus et al., 2025). In this context, measurement methods based on obtained digital photographic images have significant advantages over traditional means. The use of such methods makes it possible to simplify the measurement process significantly: all information about the distribution of such lighting parameters as luminance and illuminance within the area of interest is captured in a single frame, thereby creating a two-dimensional map. This makes it possible to analyse the luminance and illuminance of individual areas in the image quickly, from both a visual and a metrological point of view (Pierson et al., 2020; Jung and Inanici, 2018). Moreover, the use of such methods significantly reduces the time required for on-site measurements, as all information is recorded simultaneously, without the need for sequential data collection. The additional advantages are constant conditions, as all points are measured at the same time. It also provides higher reproducibility of results, as the image containing the scene can be stored for further analysis and re-evaluation.

The objective of the research was to investigate the possibility of using digital cameras to measure the luminance and

illuminance of luminous surfaces. For this purpose, camera calibration is required (Burggraaff et al., 2019) in order to use them as measuring instruments. In addition, it was necessary to determine whether the luminance values of the image areas obtained in this way remain unchanged under different exposure settings and aperture values of the camera used. Special attention should be paid to the development of a clear procedure for camera calibration, the selection of image format and colour space, as well as the methodology for verifying a number of technical parameters that may affect the effectiveness of using a camera for photometric measurements.

Analysis of scientific publications which deal with the application of digital cameras for photometric measurements demonstrates a strong scientific consensus regarding the possibility of their use in photometry due to the linear response of the sensor to the amount of incident light and the ability to read data in digital format (Hoot, 2007). The use of digital cameras as luminance meters or lux meters is possible only under the condition of their calibration (Greffier et al., 2015). In the investigations reported in the papers of other researchers, various approaches to camera calibration, image format selection, and error reduction were presented. In Pierson et al. (2020), the authors proposed the use of standard image formats, such as JPEG with settings adjusted for minimal compression, which simplifies image acquisition and processing but relies on the camera's built-in nonlinear transformations and therefore limits measurement accuracy. However, in Kurkela et al. (2017) and Greffier et al. (2015), raw digital images (raw files) which preserve the sensor's original linear response were used instead, at the cost of a more demanding processing pipeline requiring raw files handling and colour space conversion. During the image processing carried out by Pierson et al. (2020), the numerical pixel values were taken from JPEG format images without conversion to another colour space, although it was noted that the CIE 1931 XYZ colour space was used by other researchers. In Greffier et al. (2015), the CIE 1931 XYZ colour space where pixel luminance value represented by the Y coordinate was used.

In Wüller and Gabele (2007), in order to correct physical artifacts in images, noise was measured by creating a "dark frame" obtained in the absence of any light source, for example, with the lens cap on. In Greffier et al. (2015), the use of an IR filter was proposed to minimise the error. Spatial heterogeneity caused by vignetting (Kordecki et al., 2016) in Safranek and Davis (2020) and Kurkela et al. (2017) is compensated by capturing an image of a uniform light source covering the entire frame and creating the correction matrix, an empirical approach that is simple to apply, whereas in Jung and Inanici (2018), this is achieved by applying the cosine law in the calculations, which generalises without additional measurements but depends on the accuracy of the focal length and f number values reported by the camera, which are used to calculate the effective aperture diameter.

For calibration purposes, it is necessary to use a reference light source. In Andriychuk and Osadtsa (2011), a reference incandescent lamp from the "SIS" model line was used, although the exact model was not specified. However, at present, such light sources are rarely used in real lighting systems. Moreover, these light sources are characterised by the dependence of spectral power distribution on the supply voltage; consequently, changes in voltage result in variations in colour temperature (Shaw et al., 2021). Incandescent lamps also emit light exclusively in the warm light spectrum, which does not correspond to the spectral characteristics of most modern lighting systems. In the present practice of outdoor and indoor lighting, mainly semiconductor light sources (Ikonen, 2023) emitting warm-white (WarmWhite, $T = 2200$–3500 K), neutral-white (NeutralWhite, $T = 3500$–5000 K), and cold-white (ColdWhite, $T = 5000$–7000 K) colours are used, whose spectral characteristics differ significantly from incandescent lamps. In this regard, it is reasonable to use light-emitting diodes (LEDs) with different colour temperatures in calibration processes. The final step, absolute calibration, determines the relationship between the corrected relative values and physical units. This is achieved by comparing the camera response with the readings of a reference device (lux meter) and subsequently obtaining the dependences of the camera output signal on the image acquisition parameters, as proposed in Jung and Inanici (2018) and Andriychuk and Osadtsa (2011).

Although the reviewed studies provide a solid basis for camera-based photometric measurements, several questions remain open. None of the reviewed studies examined whether a single calibration model remains valid across different aperture values or whether the aperture setting itself could be a source of systematic error. Furthermore, although linearity of the sensor response is commonly assumed, a standardised procedure for determining the boundaries of the linear operating range, such as that defined by the EMVA 1288 standard, has not been applied in previous camera calibration studies for photometric purposes. In addition, calibration light sources used in earlier raw-based studies did not systematically cover the range of correlated colour temperatures characteristic of modern semiconductor lighting installations. The present study addresses these aspects by developing separate calibration models for each aperture value, applying the EMVA 1288 standard to determine the valid range of the sensor signal.

2 Camera calibration

2.1 Peculiarities of camera calibration

While setting up the camera calibration process and performing measurements, the following factors should be taken into account:

1. Camera ability to measure luminance is based on a simple and reliable physical principle. Each pixel on the

camera sensor functions as a microscopic light-sensitive element. When light strikes the pixel, it generates electrical charge. The most important aspect for measurements is that the amount of accumulated charge is linearly dependent on the amount of light incident on the pixel (Wang and Theuwissen, 2017). This linear relationship makes it possible to use a camera as a tool for the quantitative measurement of luminous flux.

2. Commercial cameras are designed to produce visually appealing images rather than for measurement purposes. The built-in signal processing unit applies a series of nonlinear transformations to the sensor output data, including gamma correction, tone curves, and colour enhancement (Burggraaff et al., 2022). These operations, which are part of the image-processing stage, convert linear sensor data into nonlinear, "display-oriented" data. The operations are irreversible and result in a loss of information, thereby limiting the use of compressed digital images (in JPEG format) for accurate measurements. Analysis of previous studies (Kurkela et al., 2017; Greffier et al., 2015; Burggraaff et al., 2019) demonstrates that employing raw files is the most appropriate approach. Work with raw files makes it possible to bypass the image processing performed by the camera's built-in processor and to gain access to data that most accurately represent the amount of light incident on the sensor.

3. Image sensors of digital cameras produce a signal that, in principle, can be correlated with luminance. However, because the converter itself usually consists of three types of sensors for perceiving the primary colours (red, green, and blue), the signal levels received by the camera from these sensors will differ even for the same luminance of the light source or image sensor illuminance. The solution of this problem is the application of CIE 1931 XYZ colour space (Molada-Tebar et al., 2024). In this colour space, the Y coordinate corresponds to luminance (Hunt and Pointer, 2011).

4. Pierson et al. (2020) and Jung and Inanici (2018) consistently indicate that minimum ISO value should be used to minimise image noise and that any calibration is valid only for a fixed set of camera settings (ISO, shutter speed, and aperture number). Verification demonstrates high laboratory accuracy, with errors ranging from 1.9 % to 5 %; however, the field error increases to ~ 20 % due to external environmental conditions (Greffier et al., 2015).

5. In practice, digital cameras first convert linear raw-RGB data into colorimetric space using a 3×3 matrix before applying the nonlinear "final" processing. Consequently, the theoretically correct approach is to convert the linear raw RGB image data directly into the CIE 1931 XYZ colour space and then extract the Y coordinate, which by definition is equal to the pixel luminance.

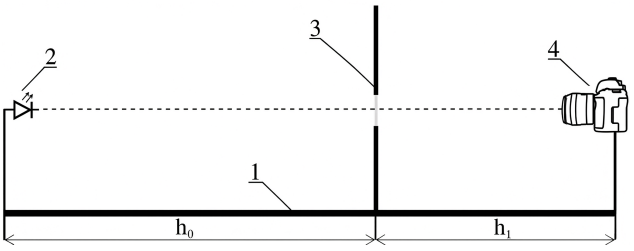


Figure 1. Schematic diagram of the calibration setup: 1 – photometric bench, 2 – light source, 3 – screen, 4 – camera.

It is important that most studies assume the absence of oversaturated data in one of the three colour channels. This is due to the disruption of the linear luminance display when at least one of the channels is overloaded (Czech et al., 2023). The conversion matrix for converting raw RGB image data to CIE 1931 XYZ is provided by the camera manufacturer as metadata in each raw image.

2.2 Camera calibration methodology

In order to establish the relationship between the luminance values of the investigated surfaces and the Y coordinate in the XYZ system of digital image elements of these surfaces, the camera was calibrated using methods similar to that described by Andriychuk and Osadtsa (2011). The calibration scheme is presented in Fig. 1. On the photometric bench 1, the light source 2 and camera 4 were located in such a way that they were aligned along the same optical axis, perpendicular to the surface of the screen 3 with diffuse transmission. The distance between the light source and the screen was $h_0 = 1.3$ m, whereas the distance between the screen and the camera was $h_1 = 0.6$ m. To prevent extraneous light from entering the camera lens, a limiting aperture covering the screen with a circular hole 10 cm in diameter was used. The calibration and measurements were carried out in a room with ceiling, wall, and floor reflectance coefficients close to zero. Changing the illumination of the screen surface from the side of the light sources, and therefore its luminance in the direction of the camera, was carried out by changing the luminous flux of the light sources due to changing their supply current.

Screen luminance control was implemented by changing the current supplied to the light sources using a variable resistance box and ammeter connected in series with the circuit, which was powered by a constant voltage source. The current was used only as a convenient means of setting different luminous flux levels of the LEDs and therefore the luminance of the screen. No assumption of linearity between current and light output was required, as the resulting screen luminance was independently measured for each setting using the luminance meter.

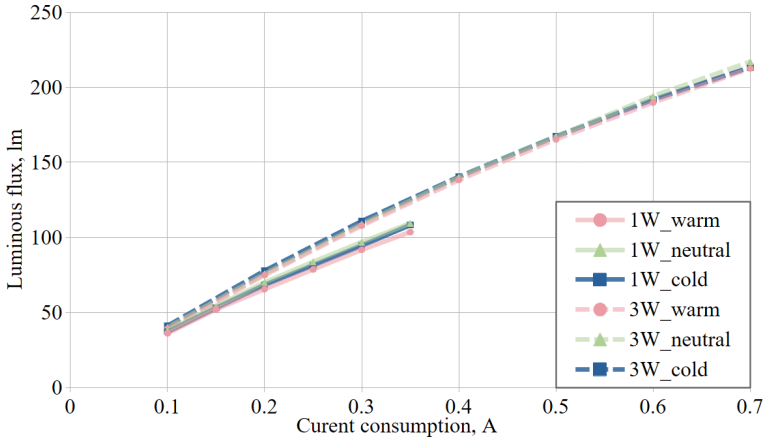


Figure 2. Dependences of LED luminous flux on the supply current.

Unlike the setup used by Andriychuk and Osadtsa (2011), warm-white, neutral-white, and cold-white "GBZ" brand light-emitting diodes (LEDs) with power ratings of 1 and 3 W were used as light sources. For 3 W LEDs, the current was changed from 0.10 to 0.70 A (nominal value) in steps of 0.10 mA, which made it possible to reach the controlled luminance range of the screen surface from 3.5 to 21.6 cd m^{-2}. In the case of 1 W LEDs, the current was varied within the range from 0.10 to 0.35 A (nominal value) with 0.05 mA step. The dependences of the luminous flux of LEDs on the current consumption is shown in Fig. 2, and their other characteristics are described in Appendix A.

Before obtaining images with the camera, the luminance of the screen in the direction of the camera was measured using "TKA-PKM" (02) luminance meter at different values of LED current and voltage. The measurement results are presented in Table 1.

Table 1. Results of luminance measurements of the diffuse-transmitting screen.

I, A	Luminance, cd m^{-2}		
	1 W, WarmWhite	1 W, NeutralWhite	1 W, ColdWhite
0.1	3.0	3.3	3.2
0.15	4.3	4.8	4.9
0.2	5.6	6.2	6.3
0.25	6.7	7.5	7.7
0.3	7.7	8.6	9.0
0.35	8.7	9.7	10.2
	3 W, WarmWhite	3 W, NeutralWhite	3 W, ColdWhite
0.1	3.9	3.6	3.5
0.2	7.5	7.3	6.9
0.3	10.8	10.7	10.0
0.4	13.8	13.6	12.8
0.5	16.4	16.4	15.4
0.6	19.1	18.7	17.6
0.7	21.6	21.1	19.7

2.2.1 Image acquisition method

Images were acquired using the camera at different values of the lens entrance aperture diameter and sensor exposure time.

Digital images of the screen on the photometric bench were acquired in the camera manual settings mode. To ensure minimal noise component in the signal, images were acquired at the minimum ISO value with all in-camera noise reduction, image enhancement, and white balance functions turned off. Similar camera settings for image acquisition were used by Pierson et al. (2020) and Jung and Inanici (2018).

During image acquisition, the camera was controlled remotely and automatically. For this purpose, a specially developed program written in the Python programming language was used, employing the GPhoto2 library (Sudomyr, 2026). The application of this approach made it possible to:

- eliminate any physical contact between the operator and the camera during image acquisition, while ensuring stable camera positioning and focusing, which is critically important for measurements,
- obtain a large number of images with different exposure parameters systematically and automatically.

The program automatically set the camera exposure time over a wide range (from 0.025 to 4 s) and adjusted the aperture value (from $f/5.6$ to $f/10$, $f/16$, and $f/20$), which is necessary for characterising the camera response across its full dynamic range during image acquisition.

The image acquisition process consisted of:

1. Setting the camera to fixed parameters (ISO) and focusing on the screen,



Figure 3. Captured screen image **(a)** and its exposure distribution **(b)**.

2. Changing the screen luminance,

3. Measuring the screen luminance,

4. Capturing the screen image in raw format.

Figure 3 shows the captured image of the screen illuminated by the 3 W cold-white LED at the nominal LED driving current, obtained by the Canon EOS 1000D camera with an exposure time of 1 s and aperture value of 5.6 (Fig. 3a), as well as the exposure distribution for this image (Fig. 3b), where for visual demonstration purposes, luminance values L were replaced by pixel luminance values Y.

The largely uniform colour across the illuminated disc shown in Fig. 3b confirms that the screen was evenly illuminated. Despite this, for higher accuracy, a smaller set of pixels was used as the area of interest, large enough to reduce the influence of the camera's sensor random noise but small enough to remain within the most evenly illuminated central zone.

2.2.2 Raw image analysis

After taking images of the screen, the next step was to extract a representative value for each sensor exposure. In order to do this, an area of interest – the centre of which corresponds to the centre of the diffuse-transmitting screen in the images – was defined. The area of interest is defined as a circular area of the image consisting of a set of pixels bounded by the circle of the given radius, for which illuminance values on the image sensor are averaged for subsequent analysis. The use of the area of interest makes it possible to isolate the area whose luminance is measured by the luminance meter. The radius of the area of interest was determined by searching for the image that showed the first signs of photo oversaturation, and the radius of the smallest circle of oversaturation was chosen as the radius of the area of interest, which was 50 pixels. This area was assumed to be uniformly illuminated only within the selected central region of interest. As shown in Fig. 3b, the central part of the raw-derived luminance distribution is nearly uniform, whereas the edge variations are related to pixel crosstalk at the boundary between the illuminated screen and the limiting aperture. Because this effect is confined to the edge of the disc, it does not affect the area of interest, which was deliberately positioned well within the uniformly illuminated central region. Further averaging of the luminance values, namely the Y coordinates, of all pixels within the area of interest significantly reduced the influence of random noise of each individual sensor pixel and provided more accurate pixel luminance value for further calculations. Further analysis of the acquired raw files was performed using a separate Python program from the same software package (Sudomyr, 2026), with the main functionality for handling raw files provided by the rawpy library, which serves as an interface to the basic LibRaw library (Riechert, 2025). The use of this library makes it possible to load raw files directly in the selected colour space without intermediate conversions. At this stage, pixel data in the CIE 1931 XYZ colour space were extracted from the area of interest. For this purpose, a specific set of parameters of the raw file loading function rawpy.imread was used:

1. output_color=rawpy.ColorSpace.XYZ – CIE 1931 XYZ colour space selection.

2. gamma= (1.0, 1.0) – gamma correction disabled.

3. no_auto_bright=True – automatic brightness adjustment turning off.

4. no_auto_scale=True – disabling automatic stretching of pixel values to the maximum 16-bit range.

5. use_camera_wb=False and use_auto_wb=False – disabling both built-in and automatic white balance.

6. user_wb = [1.0, 1.0, 1.0, 1.0] – applying the neutral white balance multiplier to avoid any scaling of individual colour channels before converting to the selected colour space.

7. demosaic_algorithm=rawpy.DemosaicAlgorithm.LINEAR – selection of the linear demosaicing algorithm (Boccuto et al., 2024).

8. output_bps=16 – selection of 16-bit pixel value expansion to preserve the full dynamic range of the sensor output data.

This carefully controlled process of extracting the required pixel data from raw files makes it possible to obtain unaltered data without image enhancement, which are the best ones for subsequent photometric calculations. At the same time, the camera settings – namely the exposure time, aperture number (f number), and focal length settings for each captured image, which are required for calculations – were programmatically read from the raw files metadata.

2.2.3 Analysis of calibration results

The next step was to establish the relationship between the screen luminance and the exposure of pixels in the area of interest on the sensor.

Exposure H was determined based on the following formula:

$$H = E_{\text{is}} \cdot t, \tag{1}$$

where E_{is} is illuminance of image sensor in area of interest and t is exposure time.

The illuminance of each individual pixel of the image sensor was calculated based on Eq. (9) (Andriychuk and Osadtsa, 2011):

$$E_{\text{p}} = \tau \cdot L \cdot \frac{\Delta S_{\text{la}} \cdot h_2^2}{\left(h_2^2 + l_2^2\right)^2}, \tag{2}$$

where τ is optical transmittance coefficient, L is screen luminance, ΔS_{la} is the area of the lens aperture, h_2 is focal length, and l_2 is distance from the image sensor centre to the pixel.

As the aperture number is the ratio of the focal length to the diameter of the lens aperture, the lens aperture area was calculated using the following formula:

$$\Delta S_{\text{la}} = \pi \cdot \frac{h_2^2}{4 \cdot N^2}, \tag{3}$$

where N is the f number.

Substituting Eq. (3) into Eq. (2) results in

$$E_{\text{p}} = \frac{\tau \cdot L \cdot \pi \cdot \cos^4\theta}{4 \cdot N^2}, \tag{4}$$

where θ is the angle between the direction of the light and the normal to the sensor for vignetting correction (Siew, 2017; Bal and Palus, 2023).

Substituting Eq. (4) into Eq. (1) results in

$$H_{\text{is}} = t \cdot E_{\text{is}} = t \cdot \frac{\tau \cdot L \cdot \pi \cdot \cos^4\theta}{4 \cdot N^2}. \tag{5}$$

Empirical analysis of the data showed that the linear relationship between the calculated exposure H_{is} and the obtained Y value is maintained only within a limited range, as shown in Fig. 4a. According to the EMVA 1288 standard, deviations from linearity at low signal levels are associated with the dominance of dark noise, resulting in the insufficient signal-to-noise ratio for the correct use of these data (Jähne, 2010). In this area, measurements are characterised by significant relative errors. As the signal level increases, the transition into the operating range is observed, where the linear dependence is observed, which meets the requirements of the EMVA 1288 standard for correct photometric measurement. In order to determine the minimum signal level at which the correct data can be used reliably, the approach consistent with the EMVA 1288 standard was applied. According to this standard, the lower limit of the operating range is defined by the transition point from the dark-noise-dominated levels to the photon noise levels. The minimum digital signal value Y can be defined as

$$Y_{\text{min}} = K \cdot \sigma_{\text{y.dark}}^2, \tag{6}$$

where $K = 12.876\,\text{e}^-/\text{DN}$ is the gain coefficient for the Canon EOS 1000D camera at ISO 100 and $\sigma_{\text{y.dark}}$ represents the standard deviation of the dark noise, which is 1.709 DN (Claff, 2026).

With a further increase in exposure, linearity is disrupted, due to the approaching of the sensor saturation level and overloading of individual colour channels. To remove this nonlinearity, where at least one of the colour channels exceeded 99 % of its maximum possible level, data were excluded from further analysis, as these data do not meet the linearity conditions.

To ensure the accuracy and reliability of the calibration, data from all images that violated linearity were excluded from further analysis and were not used in the calibration.

After filtering the data in order to include only the linear range of the sensor response, the relationship between the calculated exposure H and the calculated Y coordinate was analysed. After analysis of the measurements obtained for 3 and 1 W LED light sources with the same correlated colour temperature, it was found that their data could be combined into a single dataset. Although, in theory, different LED power can result in differences in the spectral uniformity of the emission, such an effect is not observed in the analysed data. This, in turn, justifies consideration of 3 and 1 W LEDs of the same emission colour as equivalent in terms of photometric characteristics within the limits of the carried out measurements and combining their data for use within a single model.

However, during the analysis it was found that although a linear correlation was observed for the luminance datasets of the area of interest obtained at the same f number, this linearity was broken when data corresponding to different f number values were combined. Therefore, the data were grouped into separate linear trends for each f number value, as shown in Fig. 4b. This phenomenon indicates the presence of a systematic error associated with the aperture set-

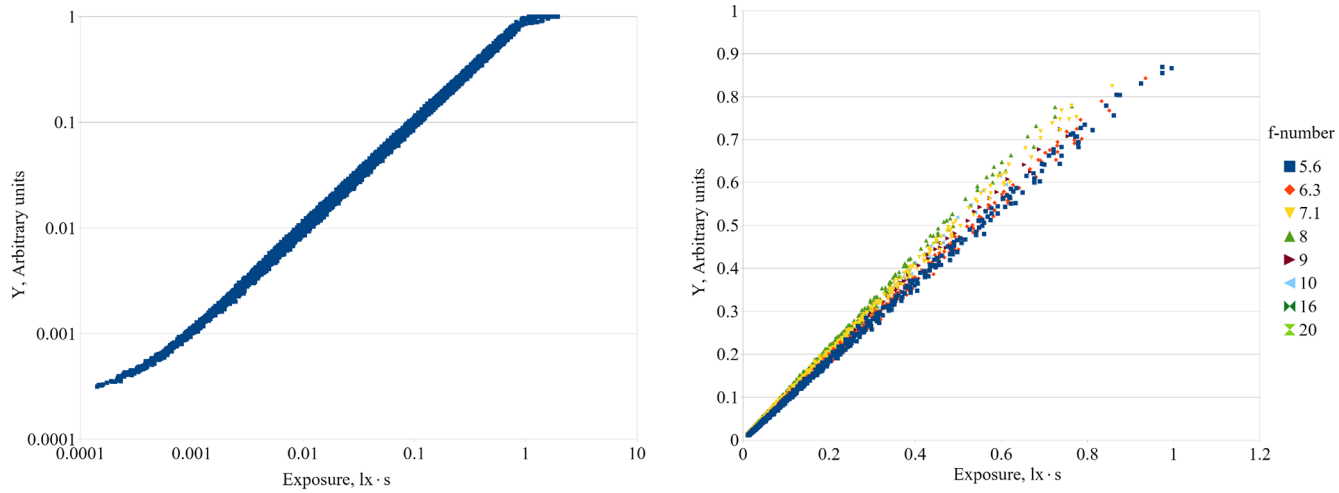


Figure 4. Plot of exposure versus Y value for all calibration images **(a)** and for filtered data divided by f number **(b)**.

ting. This can be explained by mechanical inaccuracies in the lens diaphragm mechanism. Although f numbers are standardised theoretical ratios, their physical implementation in mass-produced lenses may exhibit deviations due to manufacturing tolerances, inaccuracies of the stepper motor controlling the aperture blades, or mechanical wear. Another reason for this phenomenon could be the insufficient accuracy of the focal length value recorded in raw files by the camera. Taking into account this discrepancy, constructing a single universal model for all f number values can result in significant errors. Therefore, a separate model was developed for each f number value. This approach treats each f number setting as a unique configuration of the measurement system. A comparison of the universal model and models for each f number is presented later in the paper, and the detailed datasets and the spreadsheet used to calculate these calibration coefficients are provided in the Supplement.

2.2.4 Calibration coefficient calculation

After determining the linear range of the sensor and identifying the dependence of the system response on the screen luminance, the next step was to obtain analytical dependences of the Y coordinate of the images on the image sensor exposures. This stage is critically important, as it converts a set of empirical data into the operating measurement tool and provides a quantitative assessment of its accuracy.

To determine the calibration coefficients, the least squares method was applied to the logarithmically transformed data. In particular, the initial model is as follows:

$$Y = a \cdot H^b \tag{7}$$

and was transformed into the linear form by applying a logarithmic transformation, which made it possible to use regression analysis techniques to estimate the model parameters

Table 2. Numerical values of the calculated coefficients a and b.

	f number	b	a	R^2
Models for each f number value	5.6	1.0036752	0.9243889	0.9984840
	6.3	0.9915101	0.9298237	0.9988258
	7.1	0.9916027	1.0063373	0.9987867
	8	0.9980947	1.0639650	0.9988745
	9	0.9901105	0.9572746	0.9988532
	10	0.9876124	0.9974009	0.9987007
	16	0.9962286	1.0482531	0.9985180
	20	0.9964214	0.9747622	0.9978075
General model		0.9876049	0.9652627	0.9940196

(Warner, 2016). Despite the fact that the theoretical dependence of the image sensor response on exposure is linear, the power-law model was chosen to calculate the coefficients. This approach is due to the need to approximate data in a wide dynamic range. The application of classical linear regression results in mathematical bias, which distorts the actual physical representation of sensor linearity at low signal levels. The calculated values of the coefficients a and b are presented in Table 2.

3 Application of the camera as a photometric measurement device

3.1 Measurement of luminance and illuminance of the diffusely reflective surface

To verify the accuracy of the developed models, control measurements were carried out on diffuse-reflecting surfaces illuminated by semiconductor light sources. The general measurement scheme is shown in Fig. 5. Two source–target configurations were used. In the first configuration, a sheet of grey paper (Richter, 2018) measuring 1000×700 mm with

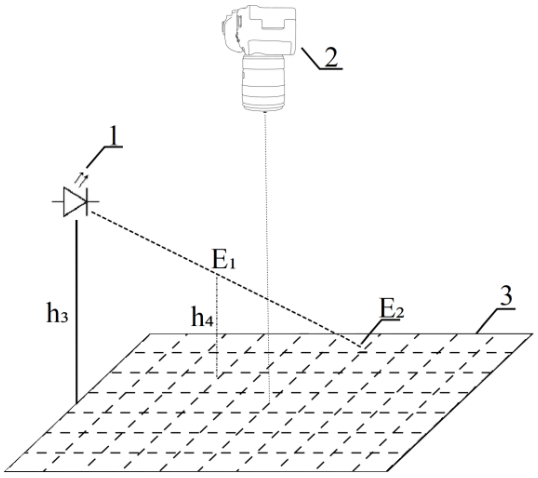


Figure 5. Scheme of obtaining control images, 1 – light source, 2 – camera, 3 – sheet of paper.

an integral reflectance coefficient of 0.28 was used as surface 3. The light source 1 was a packaged LED with a transparent lens, placed above the middle of the left edge of the sheet, creating a smooth illuminance gradient across the sheet surface. In the second configuration, a smaller sheet of dark-grey paper measuring 700×500 mm with a different integral reflectance coefficient of 0.155 was illuminated by a consumer LED lamp with a factory-integrated diffuser. In both cases, the calibrated camera 2 was placed above the centre of the sheet, and its optical axis was perpendicular to the sheet surface to maintain focus. Under these conditions, a series of raw images was captured using different combinations of exposure time and f number settings.

The choice of the non-uniform target for testing is essential. Although calibration is carried out on the uniformly illuminated screen, which allows the sensor response to be evaluated at only a single luminance level per image, the non-uniform target enables testing of the model across a wide range of luminance levels within a single frame. This provides more realistic testing, as it simulates real-world conditions where the investigated objects are rarely uniformly illuminated. This approach enables simultaneous verification of both the accuracy of the calibration itself and the spatial consistency of measurements across the entire frame, confirming the ability of the camera to function as a two-dimensional luminance meter.

It should be noted that this verification relies on the analytical $\cos^4\theta$ vignetting correction Eq. (5) rather than an empirical measurement of the camera's angular response. Rotating the camera relative to the fixed target was not performed in this study. Such a test would allow any residual spatial deviation to be attributed either to the camera and lens, if the pattern rotates with the camera, or to the scene itself, if it remains fixed relative to the target, and is left for future verification of the vignetting model.

To create a reference map of the illuminance distribution on the paper surface, measurements were performed using the lux meter function of "TKA-PKM" (02) luminance meter for the first source–target configuration, and "FLUS ET-952" for the second configuration. Measurements were carried out at grid points, with a distance of 100 mm between adjacent points, which allowed one to obtain a set of reference points with known illuminance values. In addition, during these measurements, the systematic error associated with the physical dimensions of the measuring device was corrected. Because the lux meter sensor has the finite height h_4, it was located slightly closer to the light source than the paper surface on which it was placed, which led to the systematic overestimation of the measured illuminance values. To correct this error, the inverse square law was applied; this law states that illuminance from the point source is inversely proportional to the square of the distance from the source (Mahajan, 1998).

If h_3 is the height of the LED above the paper and h_4 is the height of the lux meter sensor, then, according to the inverse square law, the relationship between the true illuminance on the paper E_2 and the measured illuminance E_1 is described by the formula

$$E_2 = \frac{E_1 \cdot (h_3 - h_4)^2}{h_3^2}. \tag{8}$$

Application of Eq. (8) to each measured point made it possible to obtain accurate reference illuminance values, which were used for subsequent comparison.

The reference map was assumed to be stable during the measurement session because the light source was kept in steady operating mode and the source–surface geometry was not changed between measurements. Repeated measurements of the illuminance distribution on the paper surface were performed to ensure it remained stable during photo captures, with the measured deviation between these measurements not exceeding 1 %.

The captured control raw images were processed using the same method as in the calibration procedure with a Python-based program (Sudomyr, 2026), including conversion to the linear XYZ colour space and extraction of the luminance coordinate Y, the distribution of which is shown in Fig. 6a. To extract data corresponding to the reference measurement points, circular areas of interest were defined on each image. The positions of the area of interest centres in the images were calculated, taking into account geometric distortions and limitations in accurately preserving scale during image acquisition of the paper sheet, in order to ensure their correspondence to the physical coordinates of the measured illuminance points.

The radius of each area of interest was not chosen arbitrarily but was selected in such a way as to ensure maximum consistency with the conditions of the reference measurements. The diameter of the cosine diffuser attachment of

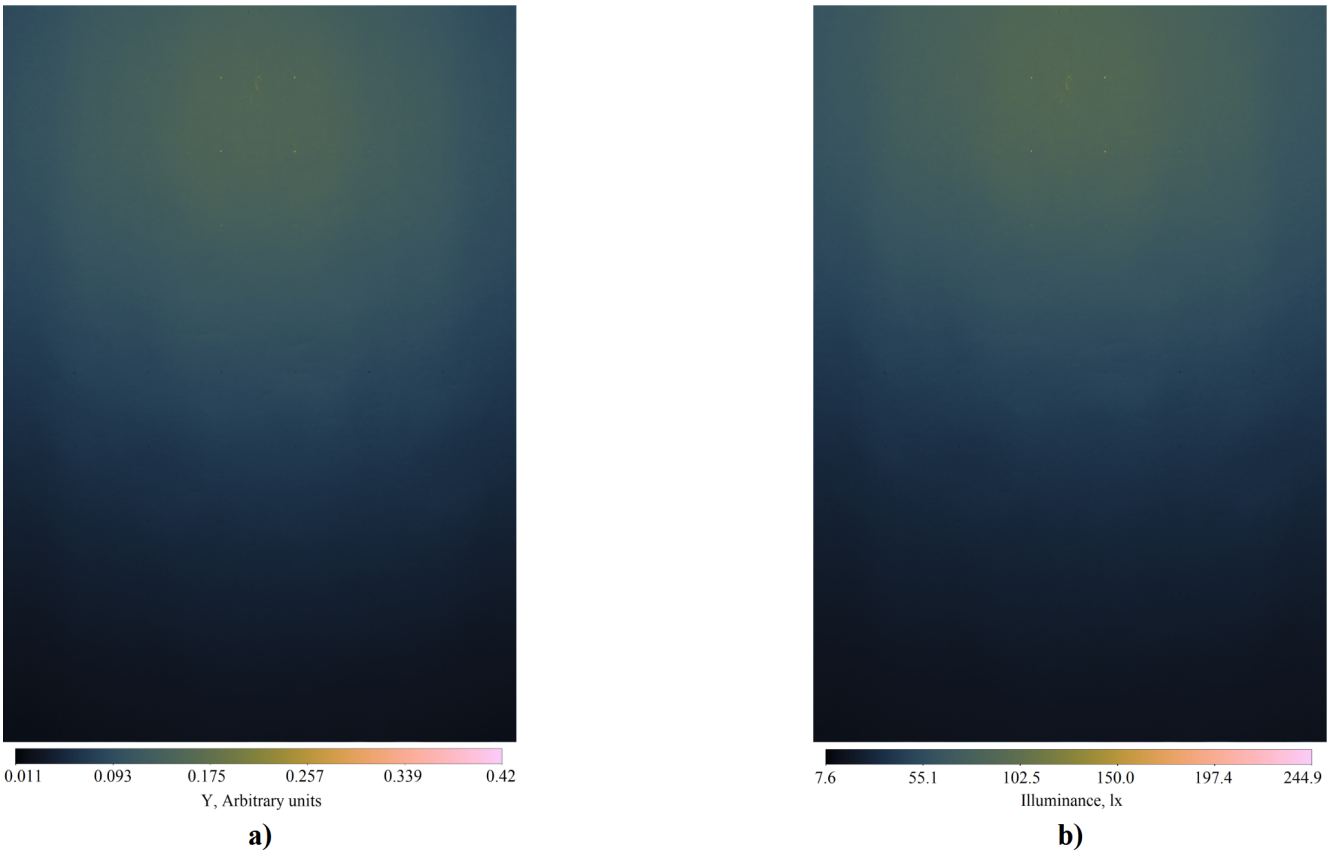


Figure 6. Distribution of the Y coordinate values **(a)** and the calculated illuminance distribution **(b)** of the control image of the paper sheet at the exposure time of 1 s and f number of 5.6.

the lux meter was 11.5 mm. At the given distance from the camera to the paper sheet and the focal length of the lens, this physical size corresponded to the diameter of 22 pixels in the image, or 380 pixels in total. Averaging the Y coordinate over this number of 12-bit raw image pixels reduces the effect of individual pixel quantisation and random noise. Setting the radius of the area of interest in this a way ensured that both the camera and the lux meter averaged the light flux over areas of equal size. This minimises discrepancies that could arise from small-scale textural inhomogeneities of the paper or noise and enables direct comparison between illuminance values obtained from the lux meter and the camera. This makes it possible to calculate the illuminance for each pixel, as it is demonstrated in Fig. 6b. Each area of interest was also checked for saturated colour channels and for minimum acceptable Y value, as in the calibration images, and invalid areas of interest were excluded.

For each area of interest in each control image, the following procedure was carried out:

1. The mean value of the Y coordinate was calculated for all pixels within the given area of interest.
2. Based on the determined coefficients a and b for each f number value or universal model, the absolute H values were calculated using the following formula:

$$H = \left(\frac{Y}{a}\right)^{\frac{1}{b}}. \tag{9}$$

3. The luminance of individual pixel of the area of interest was calculated using the following formula:

$$L = H \cdot \frac{4 \cdot N^2}{t \cdot \tau \cdot \pi \cdot \cos^4\theta}, \tag{10}$$

derived from Eq. (5).

4. Based on the obtained numerical luminance values, the illuminance of the diffusely reflecting surface was calculated using Eq. (6) (Hanus et al., 2025):

$$E = \frac{L \cdot \pi}{\rho}, \tag{11}$$

where ρ is the reflectance coefficient of the surface, measured on the target samples using an "FMSh-56" photometer.

The illuminance distribution determined by means of the Canon EOS 1000D camera over the diffusely reflecting test surface is shown in Fig. 6b.

3.2 Comparison of measurement results

The final step was the comparison of the obtained illuminance values of the diffusely reflecting surface measured with the lux meter and those derived from images captured by the camera. As an example, let us consider the comparison of the results for the surface illuminated by 3 W LED with a neutral-white colour. The values measured using the lux meter are shown in Fig. 7. The comparison was performed by calculating the deviation δE between the illuminance values obtained using the E_{dc} camera and E_{lx} lux meter according to the following formula:

$$\delta E = \frac{E_{\mathrm{dc}} - E_{\mathrm{lx}}}{E_{\mathrm{lx}}} \cdot 100\,\%. \tag{12}$$

The comparison results for the image of the diffusely reflecting surface illuminated by 3 W LED with a neutral-white correlated colour temperature and average 56.8 lx illuminance showed small discrepancy between the obtained values. For images with exposure ensuring clear visibility of the entire sheet surface, the mean deviation between illuminance values obtained using the lux meter and the camera at 1 s exposure time and 5.6 f number for 54 areas of interest using the general model was 7.85 %. At the same time, the relative deviation ranged from −15.99 %, to 2.32 %. Whereas using the model corresponding to the specific f number value, the mean deviation was 3.08 %. At the same time, the relative deviation ranged from −7.01 % to 10.16 %. The numerical values of the relative deviations between the illuminance of the diffusely reflecting surface obtained using the lux meter and the Canon EOS 1000D camera, while using the general model, are presented in Table 3, and those ones obtained using the model for specific aperture value are given in Table 4.

Similar results were also obtained for other LED light sources of different power levels and with different correlated colour temperature values.

The generalisation of the results for the primary experimental dataset, namely 21 525 areas of interest from all verification images, showed that when using models for specific aperture values, the relative deviation ranges from −25.51 % to 15.34 % with mean value of 10.47 %, whereas for the general model, the deviation varies from −24.88 % to 12.75 % with a mean value of 10.87 %. The values of absolute deviations relative to Y signal level are shown in Fig. 8.

To verify the repeatability and robustness of these findings, a second independent control measurement was performed under different experimental conditions described in Sect. 3.1. The comparison of the camera-derived illuminance values with the reference lux meter measurements for this second configuration, comprising 2277 areas of interest from all verification images of the second configuration, yielded a mean relative deviation of 9.53 % when using the general model and 9.48 % when using the model for the specific aperture value. Deviations ranged from −25.31 % to 22.11 % for general model and from −26.45 % to 27.94 % for the specific aperture value model. Consistent with the first configuration, the specific aperture model demonstrated higher accuracy in the second measurement.

Therefore, for the complete dataset, the difference between the two approaches remains relatively small; however, the improvement in accuracy is observed when using the model for specific aperture value at intermediate Y signal levels, as illustrated in the example for 1 s exposure time and 5.6 aperture value. In particular, it was determined that within the range of normalised Y signal values from 0.1 to 0.4, the specific aperture model provides higher accuracy compared to the general model, indicating its expediency for application in the mid-range signal levels.

4 Directions for further investigations

The developed methodology for calibrating digital cameras for measuring photometric parameters creates the basis for implementing autonomous outdoor lighting monitoring and control systems. A promising direction for further research is the development of compact, specialised devices equipped with pre-calibrated cameras that can be directly integrated into outdoor lighting systems or installed as separate monitoring modules. These devices can be placed on street lighting poles, building facades, or other locations for continuous monitoring of lighting parameters in urban areas, roads, pedestrian zones, and workspaces. Calibrated cameras integrated into these devices will enable the real-time automatic acquisition of luminance and illuminance distributions.

The integration of such devices with lighting control systems enables the adaptive regulation of luminous flux depending on actual conditions. The system can automatically adjust lighting intensity according to the time of day, weather conditions, availability of natural light, and user needs, ensuring compliance with regulatory requirements and optimising energy consumption.

A separate research direction should focus on the development of image-processing algorithms at the device level. It is necessary to investigate the stability of camera calibration characteristics over long-term operation under conditions of varying temperature, humidity, and other environmental factors.

Additional research is required in order to determine the possibility of using the described technology to create distributed network lighting monitoring systems at the level of entire urban areas or transport highways, where multiple autonomous devices with calibrated cameras will operate synchronously, providing a comprehensive picture of the state of the lighting environment and allowing lighting systems to be controlled based on real measured data.

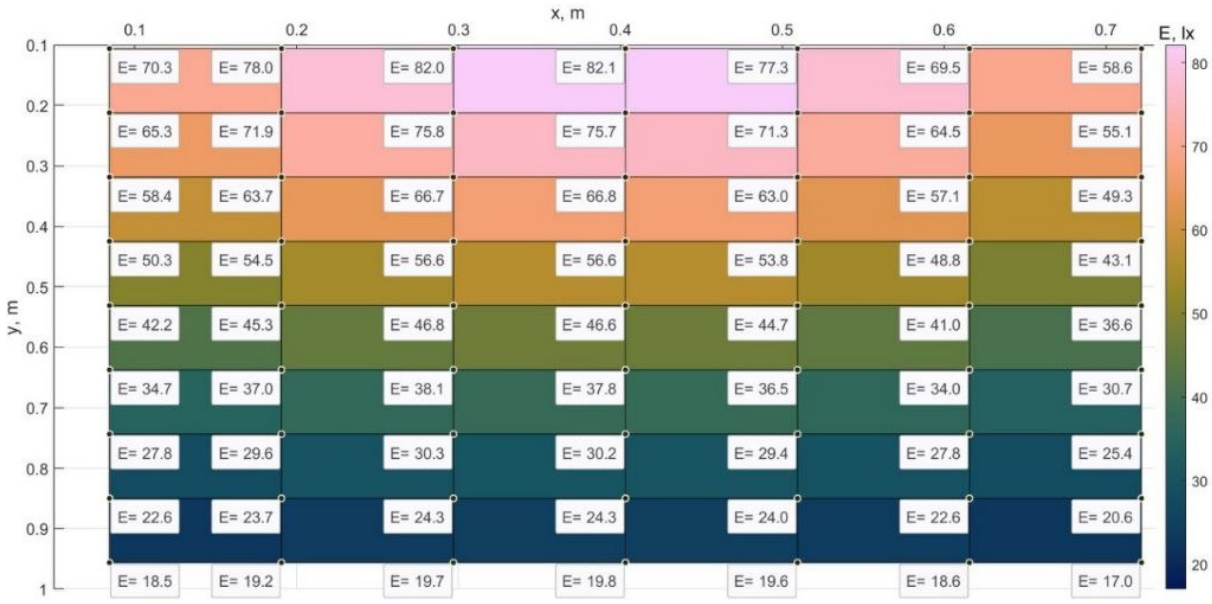


Figure 7. Illuminance values of the paper sheet measured by means of the lux meter.

Table 3. Numerical values of relative deviations obtained using the general model.

−7.37 %	−3.13 %	1.58 %	0.67 %	−5.46 %	−8.32 %
−4.50 %	−3.00 %	2.32 %	0.97 %	−2.27 %	−4.04 %
−4.22 %	−4.26 %	−2.91 %	−1.20 %	−3.72 %	−4.29 %
−5.67 %	−9.60 %	−6.15 %	−6.76 %	−7.71 %	−6.39 %
−8.02 %	−9.27 %	−8.20 %	−6.27 %	−10.40 %	−6.38 %
−10.66 %	−11.06 %	−11.10 %	−10.07 %	−11.47 %	−8.61 %
−11.25 %	−12.45 %	−10.28 %	−10.85 %	−8.68 %	−7.66 %
−12.68 %	−15.07 %	−10.45 %	−10.84 %	−9.78 %	−11.26 %
−15.99 %	−14.23 %	−10.44 %	−12.11 %	−10.37 %	−11.45 %

Table 4. Numerical values of relative deviations obtained using the model for aperture value 5.6.

0.18 %	4.47 %	9.33 %	8.36 %	1.97 %	−0.85 %
3.28 %	4.66 %	10.16 %	8.73 %	5.41 %	3.74 %
3.73 %	3.46 %	4.78 %	6.59 %	4.02 %	3.61 %
2.41 %	−2.01 %	1.57 %	0.92 %	−0.01 %	1.58 %
0.17 %	−1.36 %	−0.31 %	1.75 %	−2.60 %	1.87 %
−2.36 %	−2.94 %	−3.07 %	−1.98 %	−3.41 %	−0.19 %
−2.63 %	−4.06 %	−1.79 %	−2.40 %	−0.01 %	1.25 %
−3.79 %	−6.52 %	−1.56 %	−1.98 %	−0.77 %	−2.25 %
−7.01 %	−5.22 %	−1.13 %	−2.94 %	−0.99 %	−2.06 %

5 Conclusions

1. A methodology for calibrating digital cameras for their application as a measurement tool for photometric parameters of surfaces is presented in this paper. The proposed approach is based on careful control of the image processing, starting with the use of raw images to avoid nonlinear transformations applied by the camera's internal processor.

2. The key elements of the developed methodology are the linearisation of the sensor response by operating in the CIE 1931 XYZ colour space and the determination of the sensor operating range within which the linear relationship between exposure and digital signal is preserved in accordance with the EMVA 1288 standard.

3. A Canon EOS 1000D camera was calibrated using LED light sources of three correlated colour temperatures as reference standards, reflecting current practices in the use of lighting systems. Calibration was carried out in the luminance range from 3.5 to 21.6 cd m^{-2}, with systematic change in exposure parameters, including shutter speed from 0.025 to 4 s and aperture value from $f/5.6$ to $f/20$.

4. In order to improve measurement accuracy, it is proposed to use separate linear dependencies of the Y the

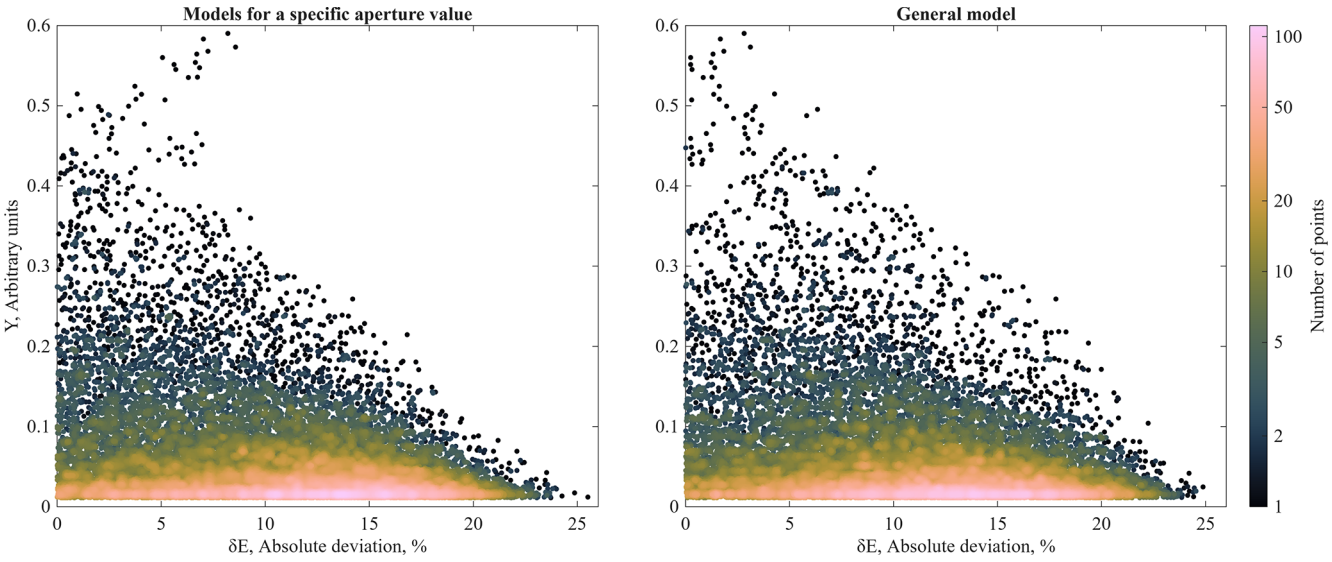


Figure 8. Graph showing the dependence of the deviation of all measured areas of interest on Y value.

coordinate of images of illuminated surfaces on the exposure at which these images are obtained for each aperture value. The coefficients of determination R^2 for all nine models exceeded 0.994, indicating a high quality of approximation of the relationships between the image sensor exposure and the Y coordinate of image luminance. In addition, vignetting compensation was taken into account by applying the cosine law, which enabled the retrieval of correct luminance values across the entire frame area.

5. The accuracy of the developed calibration models was verified by comparing illuminance measurements of the diffusely reflecting surface obtained using a calibrated camera and reference lux meter. The first experimental setup included a sheet of grey paper with 0.28 reflectance coefficient, illuminated by LED, which produced non-uniform illuminance distribution ranging from 5.5 to 92.7 lx. The comparison results for 21 525 control points showed the mean deviation of 10.47 % when using the model for specific aperture value, with a maximum deviation of −25.51 %. For comparison, the application of general model constructed on all calibration data simultaneously resulted in a mean deviation of 10.87 %, with a maximum of −24.88 %. The second experimental setup included a sheet of dark-grey paper with a 0.155 reflectance coefficient, illuminated by a consumer LED lamp, which produced a non-uniform illuminance distribution ranging from 41.3 to 654.4 lx. The comparison results for 2277 control points showed a mean absolute deviation of 9.48 % when using the model for specific aperture value, with a maximum deviation of 27.94 %. For comparison, the application of a general model constructed on all calibration data simultaneously resulted in a mean absolute deviation of 9.53 %, with maximum of −25.31 %. However, at normalised Y signal levels ranging from 0.1 to 0.4, the model constructed for specific aperture value provides higher accuracy compared to the general one.

6. The developed methodology makes it possible to transform a commercial digital camera into two-dimensional measurement device capable of simultaneously recording the luminance distribution across the entire surface of the object and calculating surface illuminance under the condition of the known reflectance coefficient. This provides a significant reduction in the labour intensity of photometric measurements of large objects and surfaces compared to traditional methods of point measurements with a luminance meter and a lux meter. The technology can be used to audit lighting systems, control the light environment of work areas and road surfaces, and develop automated systems for monitoring and controlling outdoor lighting using compact devices based on calibrated cameras.

Appendix A

Spectral and colorimetric measurements of the LEDs used for calibration in this study were carried out by means of an EVERFINE HAAS-1200 spectroradiometer in the photometric laboratory of OSP Corporation VATRA LLC. The correlated colour temperature values of LED emissions, as well as their chromaticity coordinates, are presented in Table A1, with the spectral composition for each LED shown in Fig. A1.

The deviations of correlated colour temperature δT, and the chromaticity coordinates Δx, Δy and Δxy from the cor-

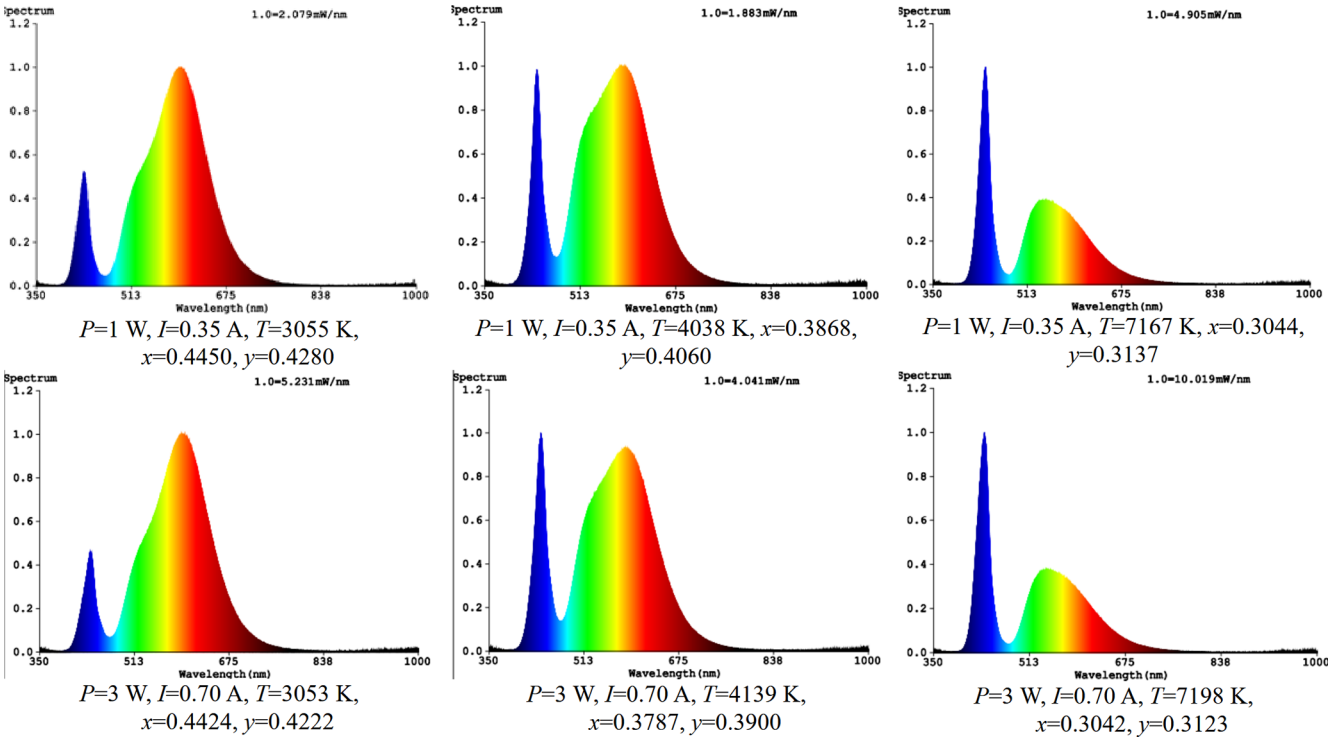


Figure A1. Spectral composition of LED radiation at nominal supply current values.

responding values when the LEDs are powered by the nominal current were calculated using the following:

$$\delta T = \frac{T_{\text{nom}} - T}{T_{\text{nom}}} \cdot 100\,\%, \tag{A1}$$

$$\Delta x = x_{\text{nom}} - x, \Delta y = y_{\text{nom}} - y, \tag{A2}$$

$$\Delta xy = \sqrt{\Delta x^2 + \Delta y^2}, \tag{A3}$$

where T_{nom}, x_{nom}, and y_{nom} are numerical values of correlated colour temperature and chromaticity coordinates at nominal values of LED supply current.

It is evident from the calculation results presented in Table A1 that the deviation of the correlated colour temperature with changes in the supply current does not exceed 8.77 %, with a corresponding chromaticity shift not exceeding $\Delta xy = 0.018$.

Table A1. Colorimetric measurement results.

I, A	T, K	δT, %	x	y	Δx	Δy	Δxy
1 W, WarmWhite							
0.35	3055	0.00	0.4450	0.4280	0.0000	0.0000	0.0000
0.30	3057	−0.07	0.4452	0.4286	−0.0002	−0.0006	0.0006
0.25	3058	−0.10	0.4454	0.4293	−0.0004	−0.0013	0.0014
0.20	3061	−0.20	0.4456	0.4301	−0.0006	−0.0021	0.0022
0.15	3065	−0.33	0.4459	0.4311	−0.0009	−0.0031	0.0032
0.10	3069	−0.46	0.4461	0.4322	−0.0011	−0.0042	0.0043
3 W, WarmWhite							
0.70	3053	0.00	0.4424	0.4222	0.0000	0.0000	0.0000
0.60	3047	0.20	0.4431	0.4230	−0.0007	−0.0008	0.0011
0.50	3042	0.36	0.4439	0.4239	−0.0015	−0.0017	0.0023
0.40	3036	0.56	0.4448	0.4250	−0.0024	−0.0028	0.0037
0.30	3034	0.62	0.4454	0.4261	−0.0030	−0.0039	0.0049
0.20	3032	0.69	0.4461	0.4272	−0.0037	−0.0050	0.0062
0.10	3032	0.69	0.4468	0.4286	−0.0044	−0.0064	0.0078
1 W, NeutralWhite							
0.35	4038	0.00	0.3868	0.4060	0.0000	0.0000	0.0000
0.30	4035	0.07	0.3871	0.4068	−0.0003	−0.0008	0.0009
0.25	4028	0.25	0.3876	0.4078	−0.0008	−0.0018	0.0020
0.20	4024	0.35	0.3882	0.4089	−0.0014	−0.0029	0.0032
0.15	4017	0.52	0.3887	0.4100	−0.0019	−0.0040	0.0044
0.10	4012	0.64	0.3893	0.4114	−0.0025	−0.0054	0.0060
3 W, NeutralWhite							
0.70	4139	0.00	0.3787	0.3900	0.0000	0.0000	0.0000
0.60	4125	0.34	0.3795	0.3913	−0.0008	−0.0013	0.0015
0.50	4109	0.72	0.3804	0.3927	−0.0017	−0.0027	0.0032
0.40	4092	1.14	0.3816	0.3945	−0.0029	−0.0045	0.0054
0.30	4082	1.38	0.3824	0.3962	−0.0037	−0.0062	0.0072
0.20	4068	1.72	0.3835	0.3982	−0.0048	−0.0082	0.0095
0.10	4055	2.03	0.3845	0.4002	−0.0058	−0.0102	0.0117
1 W, ColdWhite							
0.35	7167	0.00	0.3044	0.3137	0.0000	0.0000	0.0000
0.30	7110	0.80	0.3050	0.3149	−0.0006	−0.0012	0.0013
0.25	7054	1.58	0.3056	0.3163	−0.0012	−0.0026	0.0029
0.20	6986	2.53	0.3063	0.3179	−0.0019	−0.0042	0.0046
0.15	6913	3.54	0.3071	0.3199	−0.0027	−0.0062	0.0068
0.10	6811	4.97	0.3083	0.3224	−0.0039	−0.0087	0.0095
3 W, ColdWhite							
0.70	7198	0.00	0.3042	0.3123	0.0000	0.0000	0.0000
0.60	7135	0.88	0.3049	0.3138	−0.0007	−0.0015	0.0017
0.50	7049	2.07	0.3058	0.3158	−0.0016	−0.0035	0.0038
0.40	6961	3.29	0.3067	0.3181	−0.0025	−0.0058	0.0063
0.30	6859	4.71	0.3079	0.3207	−0.0037	−0.0084	0.0092
0.20	6730	6.50	0.3094	0.3241	−0.0052	−0.0118	0.0129
0.10	6567	8.77	0.3115	0.3291	−0.0073	−0.0168	0.0183

Code and data availability. The extracted numerical data retrieved from the raw photos and used for all calculations and validations are provided in the Supplement. Specifically, the Supplement contains spreadsheets with data retrieved from calibration photos for each LED, the coefficient calculation spreadsheet, data retrieved from validation photos, and the validation calculations. The original raw image files are available from the authors upon request due to the excessively large file size. All software code used in this work is available in a public repository and can be accessed at https://doi.org/10.5281/ZENODO.19430704 (Sudomyr, 2026).

Supplement. The supplement related to this article is available online at https://doi.org/10.5194/jsss-15-209-2026-supplement.

Author contributions. YO developed the concept of this work and designed the experiments. VS performed the experiments and developed the code. YO and VS conducted the data analysis and prepared the paper.

Competing interests. The contact author has declared that none of the authors has any competing interests.

Disclaimer. Publisher's note: Copernicus Publications remains neutral with regard to jurisdictional claims made in the text, published maps, institutional affiliations, or any other geographical representation in this paper. The authors bear the ultimate responsibility for providing appropriate place names. Views expressed in the text are those of the authors and do not necessarily reflect the views of the publisher.

Acknowledgements. The authors express their gratitude to OSP Corporation VATRA LLC for providing the opportunity to carry out spectral and colorimetric measurements of LEDs used in this research.

Review statement. This paper was edited by Bernhard Jakoby and reviewed by two anonymous referees.

References

Andriychuk, V. and Osadtsa, Y.: Vymiriuvannia svitlotekhnichnykh kharakterystyk svitnykh obiektiv za dopomohoiu fotokamer z matrychnymy optychnymy peretvoriuvachamy [The measuring of light engineering characteristics of light objects with the help of cameras with matrix optic transformers], Visnyk TNTU, 16, 126–132, https://elartu.tntu.edu.ua/bitstream/123456789/925/2/TNTUB_2011_v16_No1-Andriychuk_V_Osadtsa_Y-The_measuring_of_light_engineering_characteristics_of_light__126.pdf (last access: 12 June 2026), 2011.

Bal, A. and Palus, H.: Image Vignetting Correction Using a Deformable Radial Polynomial Model, Sensors, 23, 1157, https://doi.org/10.3390/s23031157, 2023.

Boccuto, A., Gerace, I., Giorgetti, V., Martinelli, F., and Tonazzini, A.: An Edge-Preserving Regularization Model for the Demosaicing of Noisy ColorImages, J. Math. Imag. Vis., 66, 904–925, https://doi.org/10.1007/s10851-024-01204-y, 2024.

Burggraaff, O., Schmidt, N., Zamorano, J., Pauly, K., Pascual, S., Tapia, C., Spyrakos, E., and Snik, F.: Standardized spectral and radiometric calibration of consumer cameras, Opt. Express, 27, 19075, https://doi.org/10.1364/oe.27.019075, 2019.

Burggraaff, O., Werther, M., Boss, E. S., Simis, S. G. H., and Snik, F.: Accuracy and Reproducibility of Above-Water Radiometry With Calibrated Smartphone Cameras Using RAW Data, Front. Remote Sens., 3, https://doi.org/10.3389/frsen.2022.940096, 2022.

Claff, W. J.: Photon Transfer Curve, https://photonstophotos.net/Charts/PTC.htm (last access: 3 April 2026), 2026

Czech, M., Trumpy, G., and Syed, A. R.: Do-It-Yourself LUT-based Linearization of Image Sensors, Archiving, 20, 126–130, https://doi.org/10.2352/issn.2168-3204.2023.20.1.27, 2023.

Greffier, F., Charbonnier, P., Tarel, J.-P., Boucher, V., and Fournela, F.: An automatic system for measuring road and tunnel lighting performance, HAL [preprint], https://hal.science/hal-01215842v1/document (last access: 7 May 2026), 2015.

Hanus, J., Guha, A., and Barry, A.: Beyond the Light Meter: A Case-Study on HDR-Derived Illuminance Calculations Using a Proxy-Lambertian Surface, Buildings, 15, 2131, https://doi.org/10.3390/buildings15122131, 2025.

Hoot, J.: Photometry with DSLR Cameras, Society for Astronomical Sciences Annual Symposium, 26, 67, https://www.researchgate.net/publication/234376858_Photometry_with_DSLR_Cameras (last access: 22 November 2025), 2007.

Hunt, R. W. G. and Pointer, M. R.: Measuring Colour, Wiley, https://doi.org/10.1002/9781119975595, 2011.

Ikonen, E.: Recent advances and perspectives in photometry in the era of LED lighting, Meas. Sci. Technol., 35, 021001, https://doi.org/10.1088/1361-6501/ad0de6, 2023.

Jähne, B.: EMVA 1288 Standard for Machine Vision, Optik&Photonik, 5, 53–54, https://doi.org/10.1002/opph.201190082, 2010.

Jung, B. and Inanici, M.: Measuring circadian lighting through high dynamic range photography, Light. Res. Technol., 51, 742–763, https://doi.org/10.1177/1477153518792597, 2018.

Kordecki, A., Palus, H., and Bal, A.: Practical vignetting correction method for digital camera with measurement of surface luminance distribution, SIViP, 10, 1417–1424, https://doi.org/10.1007/s11760-016-0941-2, 2016.

Kurkela, M., Maksimainen, M., Vaaja, M., Virtanen, J.-P., Kukko, A., Hyyppä, J., and Hyyppä, H.: Camera preparation and performance for 3D luminance mapping of road environments, PJF, 25, 1–23, https://doi.org/10.17690/017252.1, 2017.

Mahajan, V. N.: Optical Imaging and Aberrations, , https://doi.org/10.1117/3.265735, 1998.

Molada-Tebar, A., Verhoeven, G. J., Hernández-López, D., and González-Aguilera, D.: Practical RGB-to-XYZ Color Transformation Matrix Estimation under Different Lighting

Conditions for Graffiti Documentation, Sensors, 24, 1743, https://doi.org/10.3390/s24061743, 2024.

Pierson, C., Cauwerts, C., Bodart, M., and Wienold, J.: Tutorial: Luminance Maps for Daylighting Studies from High Dynamic Range Photography, LEUKOS, 17, 140–169, https://doi.org/10.1080/15502724.2019.1684319, 2020.

Richter, K.-P.: Calibration of exposure meter, GossenFoto- und Lichtmesstechnik GmbH, https://www.gossen-photo.de/en/calibration-of-exposure-meter/ (last access: 2 February 2026), 2018.

Riechert, M.: rawpy: Python wrapper for LibRaw, GitHub [code], https://github.com/letmaik/rawpy (last access: 17 April 2026), 2025.

Safranek, S. and Davis, R. G.: Sources of Error in HDRI for Luminance Measurement: A Review of the Literature, LEUKOS, 17, 187–208, https://doi.org/10.1080/15502724.2020.1721018, 2020.

Shaw, P.-S., Woodward, J. T., Johnson, B. C., Brown, S. W., and Yoon, H. W.: Incandescent lamp-based facility for measuring the long-term radiometric stability of spectrographs, Appl. Optics, 60, 10935, https://doi.org/10.1364/ao.444568, 2021.

Siew, R.: Relative illumination and image distortion, Opt. Eng, 56, 049701, https://doi.org/10.1117/1.oe.56.4.049701, 2017.

Sudomyr, V.: PuFF1k/DSLRCameraCalibrationAsIlluminanceMeter: New release, Zenodo [code], https://doi.org/10.5281/ZENODO.19430704, 2026.

Wang, F. and Theuwissen, A.: Linearity analysis of a CMOS image sensor, Electronic Imaging 2017, https://www.harvestimaging.com/pubdocs/213_EI2017.pdf (last access: 20 March 2026), 2017.

Warner, B. D.: A Practical Guide to Lightcurve Photometry and Analysis, Springer International Publishing, https://doi.org/10.1007/978-3-319-32750-1, 2016.

Wüller, D. and Gabele, H.: The usage of digital cameras as luminance meters, edited by: Martin, R. A., DiCarlo, J. M., and Sampat, N., SPIE Proc., 6502, 65020U, https://doi.org/10.1117/12.703205, 2007.